EFFICIENT MASKED AUTOENCODER FOR VIDEO OBJECT COUNTING AND A LARGE-SCALE BENCHMARK

Anonymous authors
Paper under double-blind review

ABSTRACT

The dynamic imbalance of the fore-background is a major challenge in video object counting, which is usually caused by the sparsity of foreground objects. This often leads to severe under- and over-prediction problems and has been less studied in existing works. To tackle this issue in video object counting, we propose a density-embedded Efficient Masked Autoencoder Counting (E-MAC) framework in this paper. To effectively capture the dynamic variations across frames, we utilize an optical flow-based temporal collaborative fusion that aligns features to derive multi-frame density residuals. The counting accuracy of the current frame is boosted by harnessing the information from adjacent frames. More importantly, to empower the representation ability of dynamic foreground objects for intra-frame, we first take the density map as an auxiliary modality to perform Density-Embedded Masked mOdeling (DEMO) for multimodal self-representation learning to regress density map. However, as DEMO contributes effective cross-modal regression guidance, it also brings in redundant background information and hard to focus on foreground regions. To handle this dilemma, we further propose an efficient spatial adaptive masking derived from density maps to boost efficiency. In addition, considering most existing datasets are limited to human-centric scenarios, we first propose a large video bird counting dataset *DroneBird*, in natural scenarios for migratory bird protection. Extensive experiments on three crowd datasets and our *DroneBird* validate our superiority against the counterparts.

1 INTRODUCTION

Video object counting aims to estimate the number of objects in video scenes and has been used in various practical applications, from traffic management to public security. It has the potential to be used in decreasing the workload of public management and protecting migratory birds. Due to the crucial role of object counting in multiple application scenarios, it has attracted broad attention in recent years with the development of computer vision.

Despite many excellent works that have been proposed over the past decades, most of these methods are based on static single-frame images (Zhang et al., 2016; Li et al., 2018) extracted from video, leading to significant loss of dynamic inter-frame information, especially for the swiftly moving targets. In practice, such as crowd or animal activity analysis, the source data is often captured in video form by surveillance cameras or drones. Unlike static single-frame images, video data is significantly dynamic in the spatial motion variations of foreground objects across adjacent time instances, thereby providing richer contextual information. Therefore, by capturing the inter-frame information between video frames, the model is qualified to better perceive dynamical targets, thereby improving the accuracy and stability of the counting performance. To this concern, some video counting methods appeared recently (Zou et al., 2019; Bai & Chan, 2021; Hossain et al., 2020), which aim to capture the dynamism between frames by employing techniques such as 3D convolutions or incorporating additional information. However, since the video data inherently suffers from the problem of redundant background information Zhou et al. (2022), extracting features of dynamic targets in multiple frames may lead to an imbalance between foreground and background information, posing challenges for the model's optimization and inference.

More recently, inspired by the unprecedented strong self-representation ability of pre-trained vision foundational models (He et al., 2021; Tong et al., 2022), researchers have injected these foundation

models into downstream vision tasks to fully exploit their representational potential. In this spirit, we present an **E**fficient **M**asked **A**utoencoder **C**ounting (E-MAC) framework for video object counting. Our E-MAC introduced optical flow-based Temporal Collaborative Fusion (TCF) to establish inter-frame relationships, constructing a pre-trained visual foundation model-based video counting framework. The optical flow between frames is used to warp the predicted density map of the adjacent frame to the current frame. Then, we perform cross-attention between the warped density map and the predicted current density map to get the final result.

However, the high dynamics of video data often lead to imbalanced optimization of the sparse foreground. Different from most existing techniques, we take the density map as an additional auxiliary modality of images and transfer the self-representation foundation model to object counting for the first time. We constructed a Density-Embedded Masked mOdeling (DEMO) that takes inputs from both the image and the density map, which performs feature interaction through the encoder and reconstructs the density map from masked image and density map. To this end, the density self-representation learning drives the regression implicitly by reconstructing the masked density maps. In addition, while the self-representation learning of density maps facilitates efficient density regression, the dynamic nature of foreground objects in video data still brings significant imbalanced challenges to optimization. Stochastic masked image modeling struggles to focus the model on extracting features from dynamic moving targets, leading to redundant background reconstruction that hinders model optimization. To handle this dilemma, we further develop a Spatial Adaptive Masking (SAM) to generate dynamic efficient masks. During training, SAM dynamically generates masks based on the correlated density map of each sample, providing valid information while filtering out redundant background details. Our framework employs a post-fusion strategy and develops a simple cross-attention module to compute the residuals between adjacent predicted density maps, and design a skip connect to add the residuals to the predicted density map of the current frame, which ultimately filters the non-dynamic objects in the background.

In this paper, we validate our E-MAC not only in human-centric scenarios but also in natural scenarios. A large-scale video bird counting dataset *DroneBird* is collected for migratory bird protection. To the best of our knowledge, DroneBird is the first video bird counting dataset that is captured from a drone's viewpoint and provides abundant annotations and rich attributions. Experimental results on three human-centric datasets and our DroneBird dataset demonstrate the superiority of our method over the competing methods. Our main contributions are summarized as follows:

- We propose a density-embedded efficient masked autoencoder counting framework for video object counting, which integrates the foundational model and takes the density map as an auxiliary modality to perform self-representation learning, effectively driving density map regression implicitly.

- We propose an efficient spatial adaptive masking method to overcome the dynamic density distribution and make the model focus on the foreground regions. It adaptively generates image masks according to the corresponding density maps, effectively addressing the problem of imbalanced fore-background.

- We propose a large-scale bird counting dataset *DroneBird* for bird activities analysis. To our knowledge, DroneBird is the first video bird counting dataset. Extensive experiments on three human-centric scenarios and our DroneBird dataset validate our superiority compared to the competing methods.

2 RELATED WORK

Object Counting. The vast majority of proposed object counting methods were commonly based on a single image. Existing counting methods (Li et al., 2018; Liu et al., 2019; Liang et al., 2022) were mainly based on density map estimation, which generated the density map from point annotations and took it as the ground truth. Most current counting methods tend to use density map regression as the pretext task of object counting since it provides more low-level supervision signals and is easier to optimize. Earlier researchers (Zhang et al., 2016; Li et al., 2018) explored improving convolutional neural network structures to enhance density regression performance by extracting multi-scale features from images. Recent methods (Ma et al., 2019; Lin et al., 2022) utilized Bayesian loss for density contribution models from point labeling, improving upon density map supervision. Additionally, researchers have integrated CNNs and Transformers to leverage the
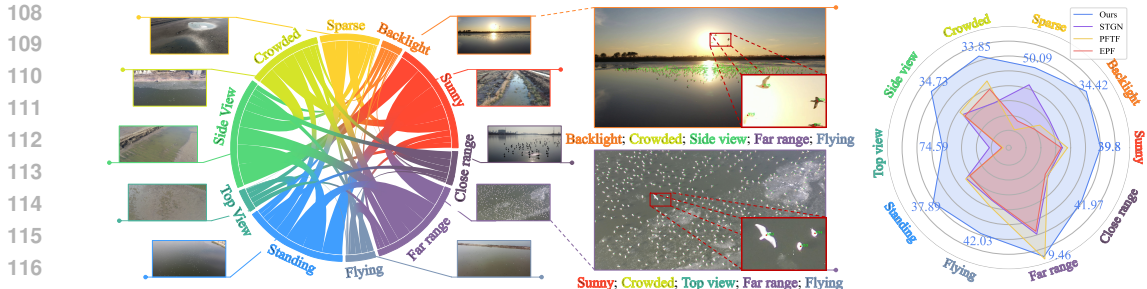
Figure 1: The chord diagram illustrates the associations between various attributes of our proposed dataset. Each attribute showcases a portion of the dataset's examples as references. We provide two zoomed-in examples for better visualization. The right part represents the experimental result of our proposed method and previous video counting method on each attribute of our DroneBird dataset.

attention mechanism (Tian et al., 2021; Liang et al., 2022). More recently, some methods introduced pre-trained foundational models to build object counting methods (Jiang et al., 2023; Kang et al., 2024), thereby counting the number of any examples. This inspired us to explore the visual foundation model based video object counting framework.

Video Object Counting. The single-frame image methods focus on spatial information from static images and neglect temporal processing, making it difficult to address the dynamic nature of video object counting tasks. The target of video object counting is to predict the number of objects in each frame of the video. For the evaluation of counting results, video counting calculates the difference between the predicted results and the ground truth for each frame, and then computes the mean absolute error (MAE) and mean squared error (RMSE) across all frame. Video object counting methods aim to leverage information from neighboring frames to enhance the estimation of the current frame. LSTM and 3D convolutions are commonly used methods for modeling temporal dependencies between frames (Zou et al., 2019; Shi et al., 2015). Unlike these implicit methods of establishing frame associations, leveraging object movement direction and optical flow information can further enhance counting accuracy (Zhu et al., 2021; Hou et al., 2023). However, existing video counting methods (Liu et al., 2020; Hou et al., 2023) mainly address temporal relationships but often neglect intra-frame dynamics of foreground regions. Additionally, the high cost of dot annotations restricts the availability of large video counting datasets, complicating effective learning of dynamic regions. Our proposed method treats counting as a density reconstruction task, incorporating self-representation learning of density maps with a dynamic spatial adaptive masking module, which significantly enhances the counting performance.

Masked Image Modeling. Masked image modeling refers to the reconstruction of the masked portion of a masked image by learning its representation. With the application of Transformer (Vaswani et al., 2017) in vision and the success of the BERT (Devlin et al., 2019) pre-training paradigm in natural language processing in recent years, masked image modeling has achieved great progress. After some enlightening work (Vincent et al., 2008; Chen et al., 2020; Bao et al., 2022), MAE (He et al., 2021) chunks the image, randomly masks out the majority of the image patches and then reconstructs them, which has achieved great success on downstream tasks. Inspired by MAE, many works (Tong et al., 2022; Bachmann et al., 2022) have begun to apply masked image prediction to diverse scenarios. Considering the strong representation ability of visual foundation models, we attempt to embed the density map to guide the masked prediction for intra-frame, performing density-driven regression from image to density map and forming an efficient self-representation learning framework for video object counting.

3 DRONEBIRD DATASET

Video object counting methods not only hold promising application prospects in human-centric activity analysis, but also possess invaluable potential in natural scenarios, such as migratory bird protection. In the scenario of counting volant species like birds, to the best of our knowledge, the existing open-source data is largely limited to discrete image data (Arteta et al., 2016; Wang et al., 2023), which makes it challenging to apply these methods to dynamic bird activity analysis scenarios. To alleviate the issue of data scarcity as well as to assist in migratory bird activity analysis, we
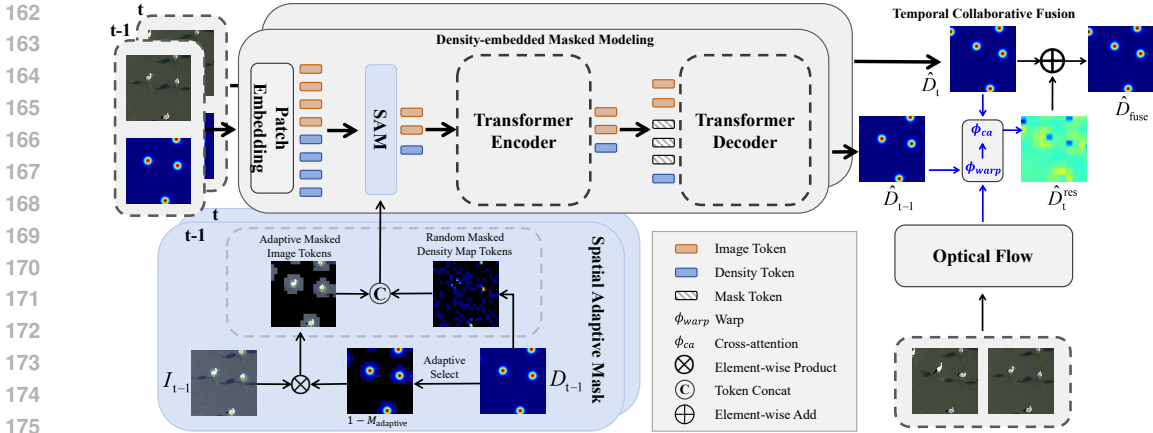
Figure 2: An overview of our E-MAC. For the temporal collaborative fusion, we use optical flow to fuse multi-frame density maps. For the density-embedded masked modeling, the image and density map are treated as multi-modal data and are fed into the transformer autoencoder for self-representation masked modeling simultaneously. The spatial adaptive masking uses the density map to balance the dynamic fore-background. During inference, the density map is fully masked.

collected a new large-scale video bird dataset called *DroneBird*. DroneBird provides point annotations for bird counting, and also provides additional trajectory annotations for further bird tracking. To the best of our knowledge, DroneBird is the first bird dataset captured in video from a drone's viewpoint and provides both point annotations and trajectory annotations.

We have collected statistics on various aspects of our DroneBird dataset and compared them with some existing datasets in Table. 4. All the videos in DroneBird are recorded at 30 frames per second with resolutions of 2160×4096 or 2160×3840. Each frame contains between 8 and 673 annotated objects, averaging 171.5 per frame. The dataset includes $3,686,409$ bird annotations and $9,389$ bird trajectories, ranging from 1 to 500 frames in length. To further investigate DroneBird, we have analyzed five main attributes of each sample, i.e., *Illumination*, *Density*, *Perspective*, *Distance*, and *Posture*. We present the distribution of these attributes and their correlation in the Fig. 3. Each arc represents a attribute, and each chord connects between two arcs, indicating that there are images that possess both attributes represented by the two arcs. For each attribute, we provide two example images in DroneBird dataset for reference. Detailed descriptions of these attributes and clearer visualization are presented in Appendix A.1.

4 METHOD

In this paper, we introduce an **E**fficient **M**asked **A**utoencoder **C**ounting (**E-MAC**) framework based on a self-representation foundation model for video object counting. The framework of our E-MAC is depicted in Fig. 2, which consists of temporal collaborative fusion (TCF), density-embedded masked modeling (DEMO), and spatial adaptive masking (SAM). We utilize optical flow to establish connections across multiple frames to capture inter-frame information. A temporal residual map is constructed by leveraging optical flow information between frames, which utilizes historical data to enhance the counting performance of the current frame. For intra-frame information, we employ density-embedded masked modeling (DEMO) and spatial adaptive masking (SAM) based on the self-representation foundation model to effectively balance the learning on foreground and background for more accurate density map estimation.

4.1 TEMPORAL COLLABORATIVE FUSION

The temporal collaborative fusion aims to integrate multiple frames for more accurate estimation. Given the frames at time t and $t-1$, each sample consists of a frame image and a density map. The samples of two frames can be described as $\mathbf{S}_t = \{I_t, D_t\}$ and $\mathbf{S}_{t-1} = \{I_{t-1}, D_{t-1}\}$, which are then fed into the DEMO for density-embedded masked modeling. Different from most existing methods, we take the density map as an auxiliary modality corresponding to the image modality.

Specifically, for a sample $\mathbf{S_t} = \{I_t, D_t\}$, the patch embedding module patchifies and embeds both the image modality and density map modality into multi-modal tokens. The SAM removes specific patches from these multi-modal tokens before the transformer encoder. After passing through the encoder, the masked positions of density map are filled with random mask tokens. The decoder then reconstructs the complete original density map based on the incomplete input information. In our framework, two temporally adjacent samples $\{\mathbf{S}_t, \mathbf{S}_{t-1}\}$ are simultaneously fed into the DEMO, where the aforementioned process is used to complete the reconstruction and generation of the predicted density maps $\{\hat{D}_t, \hat{D}_{t-1}\}$.

The reconstructed density maps $\{\hat{D}_{t-1}, \hat{D}_t\}$ are obtained by the output of DEMO. To align their spatial distributions, a pre-trained optical flow network (Sun et al., 2018) estimates the motion displacement, followed by a warp operation on $\hat{D}_{t-1}$, resulting in $\hat{D}_{t-1}^{\text{warp}}$. The cross-attention between $\hat{D}_{t-1}^{\text{warp}}$ and $\hat{D}_t$ then produces $\hat{D}_t^{\text{res}}$, representing the temporal density residuals of adjacent frames. $\hat{D}_t^{\text{res}}$ and $\hat{D}_t$ are combined via element-wise addition to output the final fused prediction $\hat{D}_{\text{fuse}}$. The TCF can be formally described by Equation 1. The fusion effect is improved by utilizing an optical flow to align information between adjacent frames. We present the whole training process in Appendix A.2 to make it easy to understand.

$$\hat{D}_{\text{fuse}} = \underbrace{\left(\phi_{\text{ca}}(\phi_{\text{warp}}(\phi_{\text{OpticalFlow}}(I_t, I_{t-1}), \hat{D}_{t-1}), \hat{D}_t) \right)}_{\text{Temporal residual density of adjacent frames}} \oplus \hat{D}_t. \tag{1}$$

4.2 DENSITY-EMBEDDED MASKED MODELING

As depicted in Fig. 2, the density-embedded masked modeling (DEMO) is a Transformer-based autoencoder. The input sample $\mathbf{S}_t$ is first divided into patches $\{\mathbf{I}_{\text{patch}}, \mathbf{D}_{\text{patch}}\}$, which are then converted into a token sequence $\mathbf{T} \in \mathbb{R}^{B \times L \times C}$ where B represents the batch size, L is the number of tokens, and C denotes the feature channels. The image I_t and density map D_t are tokenized simultaneously, then concatenated along the L dimension, where $L = \mathcal{N}_I + \mathcal{N}_D$. $\mathcal{N}_I$ and $\mathcal{N}_D$ represent the number of tokens from the image and density map modalities. SAM is a density-guided masking strategy that uses human annotations as priors. Further details are provided in Sec.4.3. It retains $\mathcal{N}_I^{\text{ret}}$ foreground tokens from image I_t and randomly keeps $\mathcal{N}_D^{\text{ret}}$ tokens from D_t, generating a new token sequence $\mathbf{T}^{\text{ret}} \in \mathbb{R}^{B \times (\mathcal{N}_I^{\text{ret}} + \mathcal{N}_D^{\text{ret}}) \times C}$.

The retained tokens are sent to the transformer encoder, while the remaining tokens are discarded and not passed into the Transformer. The output token dimension of the encoder is $B \times (\mathcal{N}_I^{\text{ret}} + \mathcal{N}_D^{\text{ret}}) \times D$. In the decoder, the retained density map tokens $\mathbf{T}_D^{\text{ret}}$ are separated from the retained token sequence $\mathbf{T}^{\text{ret}}$, where $\mathbf{T}^{\text{ret}} \in \mathbb{R}^{B \times (\mathcal{N}_I^{\text{ret}} + \mathcal{N}_D^{\text{ret}}) \times C}$ and $\mathbf{T}_D^{\text{ret}} \in \mathbb{R}^{B \times \mathcal{N}_D^{\text{ret}} \times C}$. The learnable random mask tokens are filled at the masked positions in the retained density map tokens $\mathbf{T}_D^{\text{ret}}$ as placeholders, and we use $\hat{\mathbf{T}}_D$ to represent the filled density map tokens. Cross-attention is then applied, with $\hat{\mathbf{T}}_D$ as the query and $\mathbf{T}^{\text{ret}}$ as the key and value. Then, the reconstructed density map $\hat{D}_t$ is generated by the two layer transformer, as the end of the self-representation masked modeling.

4.3 SPATIAL ADAPTIVE MASKING

The masked modeling approach discards a subset of tokens prior to the transformer encoder, utilizing the decoder to reconstruct the missing information. This process allows the model to capture the relationships between tokens. In the context of multi-modal masked modeling, it further enables the model to learn associations and interaction mechanisms across different modalities. A substantial body of research indicates that random masking strategies may introduce excessive redundant information due to the imbalanced fore-background, which is detrimental to the model's learning process. To this concern, we developed spatial adaptive masking (SAM) for efficient learning of the dynamic changing targets in videos. This strategy reduces redundant background optimization and focuses the model's attention on the image foreground, thereby improving the efficiency of self-representation learning.

For a video frame I, its density distribution D serves as the standard for delimiting the foreground and the background. The lower-left part of Fig. 2 provides a detailed illustration of the SAM. The symmetric Dirichlet distribution (Bachmann et al., 2022) is used to determine the number of retained tokens for the image modality and density map modality when generating multi-modal

masks, denoted as $\mathcal{N}_I^{\text{ret}}$ and $\mathcal{N}_D^{\text{ret}}$, respectively. We calculate the number of targets $\mathbf{V}_D^i$ in the i-th density map patch $\mathbf{D}_{\text{patch}}^i$ corresponding to each token, and $\mathbf{V}_D = \{\mathbf{V}_D^1, \mathbf{V}_D^2, \cdots \mathbf{V}_D^{\mathcal{N}_I}\}$, where $\mathbf{V}_D^i = \phi_{\text{sum}}(\mathbf{D}_{\text{patch}}^i)$. ϕ_{sum} represents the pixel-wise sum operation in each density patch (Zhang et al., 2016; Li et al., 2018), and the results represent the number of targets in the corresponding patch. To focus on the foreground, we sort the image tokens according to the number of targets $\mathbf{V}_D^i$ in the corresponding density map modality. While the foreground provides more valid information, the background should not be completely ignored. Therefore, we set a **b**ackground **r**etention **p**robability (**BRP**) $\mathcal{P}$ to introduce the background information, where BRP determines the sorting manner, in ascending order with a probability of $\mathcal{P}$ (focus on the background) or in descending order with a probability of $1 - \mathcal{P}$ (focus on the foreground). Detailed experiments of $\mathcal{P}$ are presented in the Sec. 5.4. The first $\mathcal{N}_I^{\text{ret}}$ tokens are retained to guide the masking of image I, preserving the foreground while discarding the background. Here, we denote $\mathcal{K}$ as the set of positions that should be kept, and $\mathbb{N}$ is a random variable that follows a Uniform distribution between 0 and 1, which is produced by a random number generator.

$$\mathcal{K} = \begin{cases} \texttt{argsort}_{des}(\phi_{\text{sum}}(\mathbf{D}_{\text{patch}}^i))\{1 : \mathcal{N}_I^{\text{ret}}\}, & \text{if} \quad \mathbb{N} \leq 1 - \mathcal{P}, \\ \texttt{argsort}_{asc}(\phi_{\text{sum}}(\mathbf{D}_{\text{patch}}^i))\{1 : \mathcal{N}_I^{\text{ret}}\}, & \text{otherwise.} \end{cases} \tag{2}$$

Based on this, we can obtain the spatial adaptive mask $M_{\text{adaptive}} = \{M_{\text{adaptive}}^i | 1 \leq i \leq \mathcal{N}_I\}$ for image I. For each token in position i and its corresponding mask M_{adaptive}^i, we have

$$M_{\text{adaptive}}^i = \begin{cases} 0, & \text{if} \quad i \in \mathcal{K}, \\ 1, & \text{otherwise,} \end{cases} \tag{3}$$

where 0 represent keeping and 1 represent masking. We denote the retained tokens from the image I as $\mathbf{T}_I^{\text{ret}} \in \mathbb{R}^{B \times \mathcal{N}_I^{\text{ret}} \times C}$, where $\mathbf{T}_I^{\text{ret}} = \mathbf{T}_I \otimes (1 - M_{\text{adaptive}})$ and $\mathbf{T}_I$ denotes all the tokens of image I. For the density token $\mathbf{T}_D$ corresponding to density map patch $\mathbf{D}_{\text{patch}}$, we generate a *random mask* M_{random} to retain $\mathcal{N}_D^{\text{ret}}$ tokens as $\mathbf{T}_D^{\text{ret}} \in \mathbb{R}^{B \times \mathcal{N}_D^{\text{ret}} \times C}$. These retained tokens are then concatenated to $\mathbf{T}^{\text{ret}} \in \mathbb{R}^{B \times (\mathcal{N}_I^{\text{ret}} + \mathcal{N}_D^{\text{ret}}) \times C}$ and fed into the decoder for prediction.

During inference, the density maps tokens are fully masked and removed. Only the image tokens are fed into the trained network, which is then required to fully reconstruct the density maps. In other words, we set $\mathcal{N}_D^{\text{ret}} = 0$ and $\mathcal{N}_I^{\text{ret}} = \mathcal{N}_I$.

4.4 Loss Function

In this work, we minimize the Mean Square Error (MSE) to ensure that both multi-frame fused density map $\hat{D}_{\text{fuse}}$ and the single-frame predicted result $\hat{D}_t$ approach the ground-truth density map D_t. To simplify the optimization of the optical flow network, we apply an MSE loss between the warped $\hat{I}_{t-1}^{\text{warp}}$ and the original image I_t:

$$\mathcal{L}_{\text{MSE}} = \frac{1}{2hw} \sum_{i=1}^{h} \sum_{j=1}^{w} \left(\hat{E}_{i,j} - G_{i,j}\right)^2, \tag{4}$$

where $\hat{E}$ and G represent the estimated vector and its ground truth. Specifically, $\hat{E}$ in $\mathcal{L}_{\text{fuse}}, \mathcal{L}_{\text{cur}}, \mathcal{L}_{\text{opt}}$ represents $\hat{D}_{fuse}, \hat{D}_t$ and $\hat{I}_{t-1}^{\text{warp}}$ respectively, and the corresponding G represents D_t, D_t and I_t. A Total Variations (TV) loss (Rudin et al., 1992) is introduced as a regular term to encourage spatial smoothness in $\hat{D}_{\text{fus}}$. TV loss can be expressed as:

$$\mathcal{L}_{\text{TV}} = \frac{1}{hw} \sum_{i=1}^{h} \sum_{j=1}^{w} \left[\left(\hat{D}_{\text{fuse}}^{i,j} - \hat{D}_{\text{fuse}}^{i-1,j}\right)^2 + \left(\hat{D}_{\text{fuse}}^{i,j} - \hat{D}_{\text{fuse}}^{i,j-1}\right)^2 \right]. \tag{5}$$

The objective loss function can be expressed as follow, where λ_1 - λ_4 are hyperparameters.

$$\mathcal{L} = \lambda_1 \mathcal{L}_{\text{fuse}} + \lambda_2 \mathcal{L}_{\text{cur}} + \lambda_3 \mathcal{L}_{\text{opt}} + \lambda_4 \mathcal{L}_{\text{TV}}. \tag{6}$$

5 Experiments

5.1 Experimental Settings

Datsets and Metrics. We conduct experiments on our DroneBird dataset and three video object counting datasets: Fudan-ShanghaiTech (FDST) (Fang et al., 2019), Mall (Loy et al., 2013) and

Table 1: Quantitative comparison between our proposed method and existing methods with metrics MAE and RMSE, lower metrics better. Further comparative results can be found in Sec. A.3.

Method	Type	Mall		FDST		VSCrowd		DroneBird	
		MAE↓	RMSE↓	MAE↓	RMSE↓	MAE↓	RMSE↓	MAE↓	RMSE↓
MCNN (Zhang et al., 2016)	Image	-	-	3.77	4.88	27.1	46.9	122.35	149.07
CSRNet (Li et al., 2018)	Image	2.46	4.70	2.56	3.12	13.8	21.1	66.11	79.33
CAN (Liu et al., 2019)	Image	-	-	-	-	-	-	70.21	92.15
MAN (Lin et al., 2022)	Image	-	-	2.79	4.21	8.3	10.4	_39.11_	_50.08_
HMoDE (Du et al., 2023)	Image	2.82	3.41	2.49	3.51	19.8	39.5	67.47	81.40
PET (Liu et al., 2023)	Image	1.89	2.46	1.73	2.27	_6.6_	11.0	45.10	52.35
Gramformer (Lin et al., 2024)	Image	1.69	2.14	5.15	6.32	8.09	15.65	49.11	65.50
EPF (Liu et al., 2020)	Video	-	-	2.17	2.62	10.4	14.6	97.22	133.01
PFTF (Avvenuti et al., 2022)	Video	2.99	3.72	2.07	2.69	-	-	89.76	101.02
GNANet (Li et al., 2022)	Video	-	-	2.10	2.90	8.2	**10.2**	-	-
FRVCC (Hou et al., 2023)	Video	_1.41_	_1.79_	1.88	2.45	-	-	-	-
STGN (Wu et al., 2023)	Video	1.53	1.97	_1.38_	_1.82_	9.6	12.5	92.38	124.67
Ours	Video	**1.35**	**1.76**	**1.29**	**1.69**	**6.0**	_10.3_	**38.72**	**42.92**

VSCrowd (Li et al., 2022) datasets. We use a fixed Gaussian kernel ($\sigma = 6$) to generate the ground-truth density map on these datasets. Following previous methods, we evaluate the counting performance by using Mean Absolute Error (MAE) and Root Mean Square Error (RMSE) fore each frame in datasets. MAE measures accuracy as MAE $= \frac{1}{n} \sum_{i=1}^{n} \left| D_i - \hat{D}_i \right|$, and RMSE measures robustness as RMSE $= \sqrt{\frac{1}{n} \sum_{i=1}^{n} \left(D_i - \hat{D}_i \right)^2}$, where n is the number of samples in datasets, D_i and $\hat{D}_i$ represent the ground truth and predicted density maps of the i-th sample, respectively.

Implementation Details. For the backbone network, the optical flow network leverages the pre-trained PWCNet (Sun et al., 2018), while the pre-trained ViT-B from MultiMAE (Bachmann et al., 2022) is used as the encoder in E-MAC. During inference, the density maps $\{D_{t-1}, D_t\}$ are fully masked, leaving the video frames $\{I_{t-1}, I_t\}$ intact, enabling the model to reconstruct the complete density map $\hat{D}_{\mathrm{fus}}$ from the input video alone. We adopt random horizontal flipping to perform data augmentation. Density maps are standardized by mean and standard deviation for better optimization. For hyperparameter settings, the model employs a linear learning rate warm-up for the first 15 epochs, followed by a cosine decay learning rate. The AdamW's weight decay is set to 0.05, and layer decay is set to 0.75 for the encoder. The mask ratio is 0.72. Empirically, to maintain a balance between foreground and background tokens, setting a small probability $\mathcal{P}$ of retaining only the background improves the model's performance for SAM. The probability $\mathcal{P}$ for spatial adaptive masking is set to 0.2. The trade-off weights $\lambda_1, \lambda_2, \lambda_3, \lambda_4$ are set to 10, 10, 1, and 20.

5.2 COMPARISONS

We compare our method with several state-of-the-art methods on our DroneBird dataset, the FDST dataset, the Mall dataset, and the VSCrowd dataset.

Mall. Mall provides video data from a fixed viewpoint in a shopping mall, where factors such as lighting are relatively controllable. On the Mall dataset, we follow the previous works (Bai & Chan, 2021; Hossain et al., 2020) for a fair comparison. The model is trained with the first 800 frames of the Mall dataset, and the rest $1,200$ frames are used as the test set. The input images are set to the size of 448×640 and the batch size is set to 3. The quantitative comparisons are reported in Table 1. Our method achieved significant advantages on MAE and RMSE metrics, which improves 4% of MAE and 2% of RMSE compared to the runner-up method FRVCC (Hou et al., 2023) based on CSRNet (Li et al., 2018). Compared to the PFTF, our method achieves significant reductions in MAE and RMSE of 55% and 53%. We compared our method to a video counting method PFTF (Avvenuti et al., 2022) and visualized the results on Mall dataset in the Fig. 3. Our method produces more clear and accurate density distributions of distant low-pixel targets, resulting in superior visualization performance. The quantitative and qualitative experimental results proved the superiority of our framework in the indoor scenarios.

FDST. The FDST dataset provides a wider range of scenarios, including various outdoor scenes, with more diverse variables compared to the Mall dataset, thus posing greater challenges. For quantitative comparison, we reported the MAE and RMSE metrics of our model and competing methods
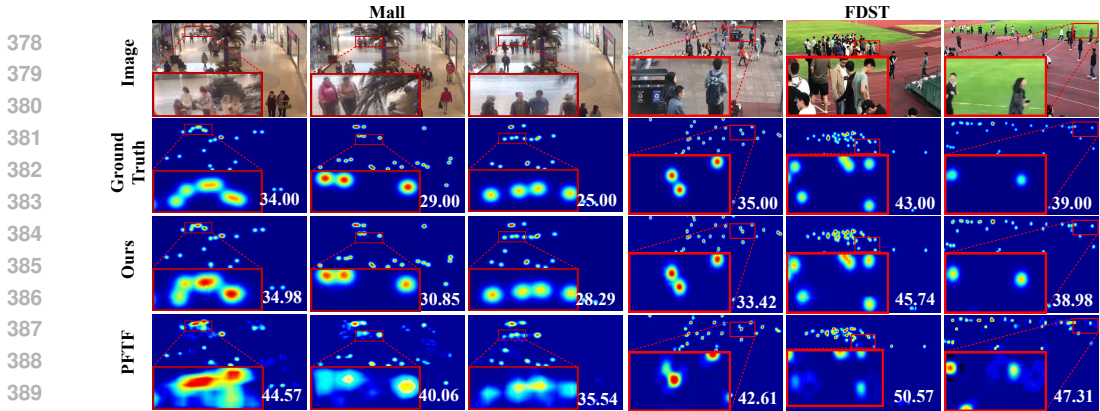
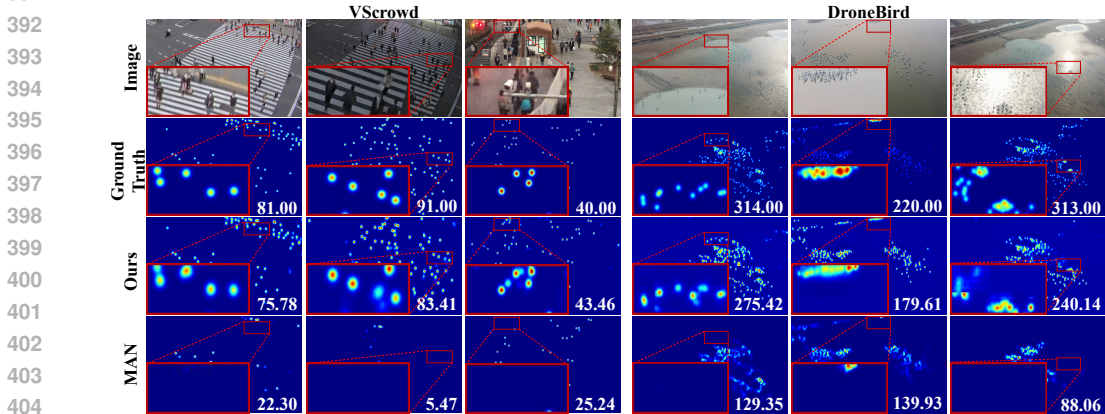Figure 3: Visualized comparisons on the FDST dataset and the Mall dataset.

Figure 4: Visualized comparisons on the VScrowd dataset and our DroneBird dataset.

on the FDST dataset in Table 1. The result shows that our method achieves the best MAE and RMSE, decreasing the two metrics of 7% compared to the runner-up method STGN (Wu et al., 2023), and 31% compared to FRVCC (Hou et al., 2023), respectively. For qualitative comparison, we visualize the predicted results of our method and the competing video counting method PFTF (Avvenuti et al., 2022) on several scenarios in Fig. 3. Our method offers better visualization effects and delivers more accurate quantitative predictions. These experimental results validate our method maintains superior performance in more complex scenarios, such as outdoor environments.

VSCrowd. VSCrowd collected more videos by using surveillance cameras or the Internet. Compared to FDST, the VSCrowd dataset provides a more diverse and complex set of outdoor scenes and presents greater challenges for video crowd counting. The evaluation results of our method and the competing method on the VSCrowd dataset are presented in Table 1. Compared to existing methods, our approach achieves superior performance on MAE and runner-up performance on RMSE metrics. Compared to the recent video counting method STGN (Wu et al., 2023), our method improves the performance by 38% in MAE and 18% RMSE, respectively. Compared to the runner-up method GNANet (Li et al., 2022), our method beat GANNet on the MAE metric and achieved competitive performance on the RMSE metric. We present detailed visualizations on the VSCrowd datasets in Fig. 4. Our method achieves accurate counting results under low-light or long-distance dense conditions compared to the previous method (Lin et al., 2022), showing the priority of our framework. These quantitative and qualitative comparison results demonstrate that our framework still possesses competitive performance in more diverse and complex outdoor scenarios.

DroneBird. Different from the previous three datasets, our DroneBird provides bird flock data from a drone's perspective, with scenes mostly consisting of open outdoor areas and exhibiting higher dynamics which pose a significant challenges for video object counting. We assessed several existing methods on ours dataset, as detailed in Table 1. Our method outperforms both recent video and image counting techniques, achieving a 58% improvement in MAE and a 66% improvement in RMSE compared to the STGN (Wu et al., 2023) method. Additionally, our approach shows enhancements in MAE and RMSE over the previous optimal method, MAN (Lin et al., 2022). For qualitative compar-

Table 2: Ablation studies on three components.

Exp.	DEMO	SAM	TCF	MAE↓	RMSE↓
I				2.45	3.22
II			✓	2.32	2.69
III		✓	✓	1.57	1.99
IV	✓		✓	1.69	2.20
V	✓	✓	✓	**1.29**	**1.69**

Table 3: Effect of each loss functions.

Exp.	$\mathcal{L}_{\text{fuse}}$	$\mathcal{L}_{\text{cur}}$	$\mathcal{L}_{\text{opt}}$	$\mathcal{L}_{\text{TV}}$	MAE↓	RMSE↓
VI	✓				1.87	2.50
VII	✓			✓	1.80	2.37
VIII	✓		✓	✓	1.60	2.03
IX	✓	✓		✓	1.39	1.77
X	✓	✓	✓	✓	**1.29**	**1.69**

ison, we compared the visualization results in multiple challenging scenarios. Our method achieves more accurate counting results of birds, even in complex areas like water reflections. The quantitative experimental results across different attributes and the visualization effects demonstrate that our framework still exhibits superior counting performance in even more complex and variable outdoor scenes from a drone's perspective, thereby highlighting the superiority of our framework. Furthermore, we conduct attribute comparisons with three competing methods (Avvenuti et al., 2022; Liu et al., 2020; Wu et al., 2023) on various attributes of the DroneBird dataset, as illustrated in Fig. 3. These experiments fully demonstrate our superiority in various complex scenarios.

5.3 ABLATION STUDY

We perform the ablation study on the FDST dataset to investigate the effectiveness of Density-embedded masked modeling (DEMO), spatial adaptive masking (SAM), and temporal collaborative fusion (TCF). We construct the same architecture as that in comparison experiments and trained for 200 epochs. The hyperparameters are set to the same as the previous experiments on the FDST dataset unless otherwise noted.

We evaluate five variants of our method to evaluate the effect of DEMO, SAM, and TCF in experiments I-V and report the quantitative results in Table 2. Exp.I denotes the baseline model of E-MAC, which performs density map regression in a pure transformer. In Exp.II, we add the optimal flow information and fusion module to construct inter-frame relationship. In Exp.III, we add the SAM based on Exp.II to perform adaptive masks. In Exp.IV, we perform the self-representation learning to Exp.II to evaluate the effect of DEMO. Notes that in Exp.IV, we randomly mask both images and density maps, while in Exp.III we only perform masks to images with our proposed SAM. In Exp.V, we simultaneously used DEMO and SAM to test the model's comprehensive performance.

Effect of `TCF`**.** We incorporated the optical flow module and fusion module into Exp.II and compared its performance with Exp.I. The results indicate that the construction of inter-frame relationships brought a performance improvement of 5% to 16% in terms of MAE and RMSE. By employing optical flow mapping, we were able to effectively leverage the inherent temporal information present in video data, enhancing the information of the current frame and improving the overall performance. Further study and visualization on TCF are presented in Appendix A.5.

Effect of `DEMO`**.** As shown in Exp.II and Exp. IV in Table 2, `DEMO` brings in 27% and 18% improvement on MAE and RMSE metrics. In Exp.V, the introduction of the self-representation learing of density maps resulted in 17% and 15% improvement in MAE and RMSE compared to Exp.III. The self-representation learning of density maps implicitly drive the regression of density maps and effectively boost the counting performance.

Effect of `SAM`**.** In Exp.III, foreground tokens from images are selected while all image tokens are selected in Exp.II. As shown in Exp.II and Exp.III, our proposed spatial adaptive masking brings an improvement of 32% in MAE and 26% in RMSE. Exp.II and Exp.III show the effect of our proposed `SAM`. Additionally, `SAM` brought 23% performance improvement to `DEMO` in Exp.V. Hyperparameter $\mathcal{P}$ is set to 0.2 in Exp.III and Exp.IV.

5.4 DISCUSSION

Loss Analysis. We conducted a detailed analysis for each loss function. We trained our model for 200 epochs, and reported the quantitative results in Table 3. Experiments VI-X correspond to the performance with different losses, showcasing the effectiveness of employing different loss functions in our proposed framework. We take Exp.VI as the baseline, which only uses $\mathcal{L}_{\text{fuse}}$ in the framework, and then gradually adds the loss term in subsequent experiments. Specifically, the addition of $\mathcal{L}_{\text{TV}}$ leads to a 4% and 5% enhancement in MAE and RMSE, respectively. In Exp.VIII, we introduce supervision through $\mathcal{L}_{\text{opt}}$, which optimizes the optical flow network by considering
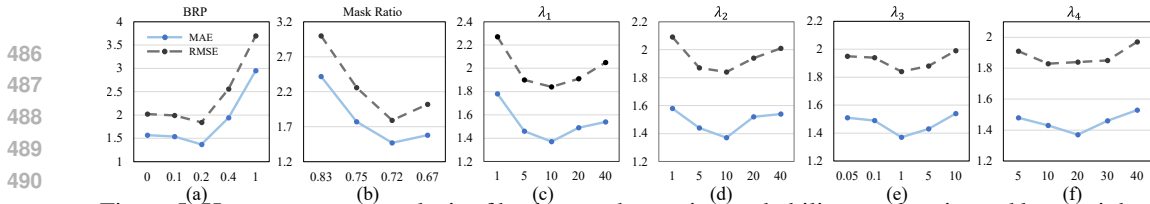
Figure 5: Hyperparameter analysis of background retention probability, mask ratio, and loss weights.

the warped previous frame. This results in 11% and 14% performance improvement compared to Exp.VII. In Exp.IX, we add the constraint of $\mathcal{L}_{\text{cur}}$, targeting the density map generated from a single frame image. Compared to Exp.VII, MAE and RMSE in Exp.IX improves 23% and 25%. Building upon Exp.VIII, Exp.X involves the addition of $\mathcal{L}_{\text{cur}}$. This leads to a significant improvement of 19% and 17% in MAE and RMSE over the performance of Exp.VII. $\mathcal{L}_{\text{cur}}$ provides a more direct constrain signal for DEMO, thus achieving more improvements compared to other loss terms.

Impact of Background Retention Probability. We have conducted an in-depth analysis for our SAM. Considering that discarding background redundant information altogether leads to imbalanced learning towards foreground, which in turn exhibits a decrease in performance. On the other hand, omissions during manual annotation could result in some counting information being present in the background. Therefore, we retain only the background of I_t during SAM with a certain probability $\mathcal{P}$. Based on Exp.V, we conduct further experiments on the choices of $\mathcal{P}$. We choose five sampling points: $0, 0.1, 0.2, 0.4$, and 1, in our experiments and compared them with the Exp.V in the ablation study. The subfigure (a) of Fig. 5 provides a more intuitive view of the final performance with respect to the probability $\mathcal{P}$. The horizontal axis indicates the probability of sorting the tokens in ascending order. We notice that the curve shows a clear downward rebound trend, and the quantitative metrics show a decline of different degrees in both four experiments compared to Exp.V. We finally choose 0.2 as the default probability in our experiments.

Impact of Mask Ratio. We conducted experiments and set the mask ratio to different values to evaluate the impact of the mask ratio on DEMO. To more clearly evaluate the impact of the mask ratio, these experiments were specifically performed on the our E-MAC without considering temporal information. The subfigure (b) of Fig. 5 shows the impact of mask ratio on counting performance. We varied the mask ratio in the range of 0.67 to 0.83, the lower the mask ratio, the more tokens entered into the model. The results show that the MAE decreases as the mask ratio decreases. However, when we set the mask ratio to 0.67, the performance of the model decreases by 7% compared to the model with a 0.72 mask ratio. We consider that a lower mask ratio can provide sufficient information to support reconstruction learning. While a mask ratio that is too low may bring in partial redundant information, which may affect the performance.

Hyperparameter Analysis. We conducted experiments on the setting of the hyperparameters $\{\lambda_1, \lambda_2, \lambda_3, \lambda_4\}$ of each loss function, as shown in subfigure (c-f)of Fig 5. We vary the weights of the remaining loss terms while fixing the weights of the other three loss terms, and the experimental results correspond to the four subfigures of Fig 5. We finally fixed the weights $\lambda_1, \lambda_2, \lambda_3, \lambda_4$ of each loss term to $10, 10, 1, 20$ in our experiments.

6 CONCLUSION

This paper aims to address the dynamic imbalance of the fore-background in video object counting. Considering the dynamic sparsity of foreground objects, we proposed a density-embedded efficient masked autoencoder counting framework. We introduced the self-representation foundation model to video object counting, which first takes the density map as an auxiliary modality and develops density-embedded masked modeling (DEMO) to drive the regression of density map estimation. To handle the infra-frame dynamic density distribution and make the model focus more on the foreground region in the self-representation learning, we proposed a simple but efficient **S**patial **A**daptive **M**asking (SAM), which dynamically generates masks depending on density maps to eliminate the effect of redundant background information and boost the performance. Furthermore, accounting for the inter-frame dynamism and utilizing the inherent temporal information in the video, we introduce the optical flow and propose a temporal collaborative fusion that learns to harness the inter-frame differences. Besides, we first proposed a new large-scale video bird dataset in the drone perspective, named DroneBird. Our DroneBird provides point and trajectory annotations in different scenes for counting and further localization and tracking tasks. Experimental results verify our superiority.

REFERENCES

C. Arteta, V. Lempitsky, and A. Zisserman. Counting in the wild. In *European Conference on Computer Vision*, 2016.

Marco Avvenuti, Marco Bongiovanni, Luca Ciampi, Fabrizio Falchi, Claudio Gennaro, and Nicola Messina. A spatio-temporal attentive network for video-based crowd counting. In *2022 IEEE Symposium on Computers and Communications (ISCC)*, pp. 1–6, 2022. doi: 10.1109/ISCC55528. 2022.9913019.

Roman Bachmann, David Mizrahi, Andrei Atanov, and Amir Zamir. MultiMAE: Multi-modal multi-task masked autoencoders. *European Conference on Computer Vision*, 2022.

Haoyue Bai and S. H. Gary Chan. Motion-guided non-local spatial-temporal network for video crowd counting, 2021.

Hangbo Bao, Li Dong, Songhao Piao, and Furu Wei. BEit: BERT pre-training of image transformers. In *International Conference on Learning Representations*, 2022. URL https://openreview.net/forum?id=p-BhZSz59o4.

Mark Chen, Alec Radford, Rewon Child, Jeffrey Wu, Heewoo Jun, David Luan, and Ilya Sutskever. Generative pretraining from pixels. In Hal Daumé III and Aarti Singh (eds.), *Proceedings of the 37th International Conference on Machine Learning*, volume 119 of *Proceedings of Machine Learning Research*, pp. 1691–1703. PMLR, 13–18 Jul 2020. URL https://proceedings.mlr.press/v119/chen20s.html.

Jacob Devlin, Ming-Wei Chang, Kenton Lee, and Kristina Toutanova. BERT: Pre-training of deep bidirectional transformers for language understanding. In Jill Burstein, Christy Doran, and Thamar Solorio (eds.), *Proceedings of the 2019 Conference of the North American Chapter of the Association for Computational Linguistics: Human Language Technologies, Volume 1 (Long and Short Papers)*, pp. 4171–4186, Minneapolis, Minnesota, June 2019. Association for Computational Linguistics. doi: 10.18653/v1/N19-1423. URL https://aclanthology.org/N19-1423.

Alexey Dosovitskiy, Lucas Beyer, Alexander Kolesnikov, Dirk Weissenborn, Xiaohua Zhai, Thomas Unterthiner, Mostafa Dehghani, Matthias Minderer, Georg Heigold, Sylvain Gelly, et al. An image is worth 16x16 words: Transformers for image recognition at scale. *arXiv preprint arXiv:2010.11929*, 2020.

Zhipeng Du, Miaojing Shi, Jiankang Deng, and Stefanos Zafeiriou. Redesigning multi-scale neural network for crowd counting. *IEEE Transactions on Image Processing*, 2023.

Yanyan Fang, Biyun Zhan, Wandi Cai, Shenghua Gao, and Bo Hu. Locality-constrained spatial transformer network for video crowd counting. *arXiv preprint arXiv:1907.07911*, 2019.

Yanyan Fang, Shenghua Gao, Jing Li, Weixin Luo, Linfang He, and Bo Hu. Multi-level feature fusion based locality-constrained spatial transformer network for video crowd counting. *Neurocomputing*, 392:98–107, 2020. ISSN 0925-2312. doi: https://doi.org/10.1016/j.neucom.2020.01.087. URL https://www.sciencedirect.com/science/article/pii/S0925231220301454.

Kaiming He, Xinlei Chen, Saining Xie, Yanghao Li, Piotr Dollár, and Ross Girshick. Masked autoencoders are scalable vision learners. *arXiv:2111.06377*, 2021.

Mohammad Asiful Hossain, Kevin Cannons, Daesik Jang, Fabio Cuzzolin, and Zhan Xu. Video-based crowd counting using a multi-scale optical flow pyramid network. In *Proceedings of the Asian Conference on Computer Vision (ACCV)*, November 2020.

Yi Hou, Shanghang Zhang, Rui Ma, Huizhu Jia, and Xiaodong Xie. Frame-recurrent video crowd counting. *IEEE Transactions on Circuits and Systems for Video Technology*, 33(9):5186–5199, 2023. doi: 10.1109/TCSVT.2023.3250946.

Ruixiang Jiang, Lingbo Liu, and Changwen Chen. Clip-count: Towards text-guided zero-shot object counting. In *Proceedings of the 31st ACM International Conference on Multimedia*, MM '23, pp. 4535–4545, New York, NY, USA, 2023. Association for Computing Machinery. ISBN 9798400701085. doi: 10.1145/3581783.3611789. URL https://doi.org/10.1145/3581783.3611789.

Seunggu Kang, WonJun Moon, Euiyeon Kim, and Jae-Pil Heo. Vlcounter: Text-aware visual representation for zero-shot object counting. In *Proceedings of the AAAI Conference on Artificial Intelligence*, volume 38, pp. 2714–2722, 2024.

Haopeng Li, Lingbo Liu, Kunlin Yang, Shinan Liu, Junyu Gao, Bin Zhao, Rui Zhang, and Jun Hou. Video crowd localization with multifocus gaussian neighborhood attention and a large-scale benchmark. *IEEE Transactions on Image Processing*, 31:6032–6047, 2022. doi: 10.1109/TIP.2022.3205210.

Yuhong Li, Xiaofan Zhang, and Deming Chen. Csrnet: Dilated convolutional neural networks for understanding the highly congested scenes. In *2018 IEEE/CVF Conference on Computer Vision and Pattern Recognition*, pp. 1091–1100, 2018. doi: 10.1109/CVPR.2018.00120.

Dingkang Liang, Xiwu Chen, Wei Xu, Yu Zhou, and Xiang Bai. Transcrowd: weakly-supervised crowd counting with transformers. *Science China Information Sciences*, 65(6):1–14, 2022.

Hui Lin, Zhiheng Ma, Rongrong Ji, Yaowei Wang, and Xiaopeng Hong. Boosting crowd counting via multifaceted attention. In *CVPR*, 2022.

Hui Lin, Zhiheng Ma, Xiaopeng Hong, Qinnan Shangguan, and Deyu Meng. Gramformer: Learning crowd counting via graph-modulated transformer, 2024. URL https://arxiv.org/abs/2401.03870.

Chengxin Liu, Hao Lu, Zhiguo Cao, and Tongliang Liu. Point-query quadtree for crowd counting, localization, and more. In *Proceedings of the IEEE/CVF International Conference on Computer Vision (ICCV)*, 2023.

Weizhe Liu, Mathieu Salzmann, and Pascal Fua. Context-aware crowd counting. In *The IEEE Conference on Computer Vision and Pattern Recognition (CVPR)*, June 2019.

Weizhe Liu, Mathieu Salzmann, and Pascal Fua. Estimating people flows to better count them in crowded scenes. In *The European Conference on Computer Vision (ECCV)*, August 2020.

Chen Change Loy, Shaogang Gong, and Tao Xiang. From semi-supervised to transfer counting of crowds. In *2013 IEEE International Conference on Computer Vision*, pp. 2256–2263, 2013. doi: 10.1109/ICCV.2013.270.

Zhiheng Ma, Xing Wei, Xiaopeng Hong, and Yihong Gong. Bayesian loss for crowd count estimation with point supervision. In *Proceedings of the IEEE International Conference on Computer Vision*, pp. 6142–6151, 2019.

Shiqiao Meng, Jiajie Li, Weiwei Guo, Lai Ye, and Jinfeng Jiang. Phnet: Parasite-host network for video crowd counting. In *2020 25th International Conference on Pattern Recognition (ICPR)*, pp. 1956–1963, 2021. doi: 10.1109/ICPR48806.2021.9412792.

Leonid I. Rudin, Stanley Osher, and Emad Fatemi. Nonlinear total variation based noise removal algorithms. *Physica D: Nonlinear Phenomena*, 60(1):259–268, 1992. ISSN 0167-2789. doi: https://doi.org/10.1016/0167-2789(92)90242-F. URL https://www.sciencedirect.com/science/article/pii/016727899290242F.

Xingjian Shi, Zhourong Chen, Hao Wang, Dit-Yan Yeung, Wai-kin Wong, and Wang-chun Woo. Convolutional lstm network: a machine learning approach for precipitation nowcasting. In *Proceedings of the 28th International Conference on Neural Information Processing Systems - Volume 1*, NIPS'15, pp. 802–810, Cambridge, MA, USA, 2015. MIT Press.

Weibo Shu, Jia Wan, Kay Chen Tan, Sam Kwong, and Antoni B Chan. Crowd counting in the frequency domain. In *Proceedings of the IEEE/CVF Conference on Computer Vision and Pattern Recognition*, pp. 19618–19627, 2022.

Deqing Sun, Xiaodong Yang, Ming-Yu Liu, and Jan Kautz. PWC-Net: CNNs for optical flow using pyramid, warping, and cost volume. In *2018 IEEE Conference on Computer Vision and Pattern Recognition*, 2018.

Ye Tian, Xiangxiang Chu, and Hongpeng Wang. Cctrans: Simplifying and improving crowd counting with transformer. *arXiv preprint arXiv:2109.14483*, 2021.

Zhan Tong, Yibing Song, Jue Wang, and Limin Wang. VideoMAE: Masked autoencoders are data-efficient learners for self-supervised video pre-training. In *Advances in Neural Information Processing Systems*, 2022.

Ashish Vaswani, Noam Shazeer, Niki Parmar, Jakob Uszkoreit, Llion Jones, Aidan N Gomez, Łukasz Kaiser, and Illia Polosukhin. Attention is all you need. *Advances in neural information processing systems*, 30, 2017.

Pascal Vincent, Hugo Larochelle, Yoshua Bengio, and Pierre-Antoine Manzagol. Extracting and composing robust features with denoising autoencoders. In *Proceedings of the 25th International Conference on Machine Learning*, ICML '08, pp. 1096–1103, New York, NY, USA, 2008. Association for Computing Machinery. ISBN 9781605582054. doi: 10.1145/1390156.1390294. URL https://doi.org/10.1145/1390156.1390294.

Hongchang Wang, Huaxiang Lu, Huimin Guo, Haifang Jian, Chuang Gan, and Wu Liu. Bird-count: a multi-modality benchmark and system for bird population counting in the wild. *Multimedia Tools and Applications*, Apr 2023. ISSN 1573-7721. doi: 10.1007/s11042-023-14833-z. URL https://doi.org/10.1007/s11042-023-14833-z.

Xingjiao Wu, Baohan Xu, Yingbin Zheng, Hao Ye, Jing Yang, and Liang He. Fast video crowd counting with a temporal aware network. *Neurocomputing*, 403:13–20, 2020.

Zhe Wu, Xinfeng Zhang, Geng Tian, Yaowei Wang, and Qingming Huang. Spatial-temporal graph network for video crowd counting. *IEEE Transactions on Circuits and Systems for Video Technology*, 33(1):228–241, 2023. doi: 10.1109/TCSVT.2022.3187194.

Feng Xiong, Xingjian Shi, and Dit-Yan Yeung. Spatiotemporal modeling for crowd counting in videos. In *2017 IEEE International Conference on Computer Vision (ICCV)*, pp. 5161–5169, 2017. doi: 10.1109/ICCV.2017.551.

Yifan Yang, Guorong Li, Zhe Wu, Li Su, Qingming Huang, and Nicu Sebe. Reverse perspective network for perspective-aware object counting. In *Proceedings of the IEEE/CVF conference on computer vision and pattern recognition*, pp. 4374–4383, 2020.

Yingying Zhang, Desen Zhou, Siqin Chen, Shenghua Gao, and Yi Ma. Single-image crowd counting via multi-column convolutional neural network. In *Proceedings of the IEEE Conference on Computer Vision and Pattern Recognition (CVPR)*, June 2016.

Joey Tianyi Zhou, Le Zhang, Jiawei Du, Xi Peng, Zhiwen Fang, Zhe Xiao, and Hongyuan Zhu. Locality-aware crowd counting. *IEEE Transactions on Pattern Analysis and Machine Intelligence*, 44(7):3602–3613, 2022. doi: 10.1109/TPAMI.2021.3056518.

Pengfei Zhu, Tao Peng, Dawei Du, Hongtao Yu, Libo Zhang, and Qinghua Hu. Graph regularized flow attention network for video animal counting from drones. *IEEE Transactions on Image Processing*, 30:5339–5351, 2021. doi: 10.1109/TIP.2021.3082297.

Zhikang Zou, Huiliang Shao, Xiaoye Qu, Wei Wei, and Pan Zhou. Enhanced 3d convolutional networks for crowd counting. *arXiv preprint arXiv:1908.04121*, 2019.